Schweizerische Eidgenossenschaft
Confédération suisse
Confederazione Svizzera
Confederaziun svizra

Eidgenössisches Departement für
Umwelt, Verkehr, Energie und Kommunikation UVEK

Bundesamt für Energie BFE

Final report 16.03.2022

Design Methodology for Supervisory Control of Vehicle Propulsion Systems, Simulation and Test Bench Studies (MERFAS)

Auftraggeber:
Bundesamt für Energie BFE
CH-3003 Bern
www.bfe.admin.ch

Auftragnehmer:
FPT Motorenforschung AG
Schlossstrasse 2
9320 Arbon
www.fpt-motorenforschung.ch

Autoren:
Prof. Dr. Christopher Onder, ETHZ, IDSC onder@idsc.mavt.ethz.ch
Dr. Manuel Gehlen, FPT Motorenforschung AG, manuel.gehlen@ivecogroup.com
Johannes Ritzmann, ETHZ, IDSC jritzman@idsc.mavt.ethz.ch

BFE-Bereichsleiter: Luca Castiglioni
BFE-Programmleiter: Luca Castiglioni
BFE-Vertragsnummer: SI/501742-01

Table of Content

1 Introduction and Project Goal

Todays’ Diesel-based propulsion systems power a wide range of vehicles, giving rise to a highly diversified product portfolio. To limit the development costs for such a vast portfolio, these systems are designed in a modular fashion and consist of various sophisticated and well-understood components such as engines, gearboxes, aftertreatment systems, etc. Ensuring compliance with legislative limitations while reducing the fuel consumption is no longer possible by optimizing the single system components alone, given their high degree of technical maturity. Further improvement of system performance therefore requires the exploitation of the interactions between the components by means of a holistic control approach.

This project aims at developing a transferable methodology for the layout and a framework for the implementation of predictive supervisory controllers targeting the optimal system-wide coordination of the major energy flows and components. These supervisory controllers will continuously define the set points for all relevant components at every point in time, relying on well-designed component controllers to perform their tasks. An example of such a system is a Diesel-electric hybrid vehicle, where the operation of the electric machine has an impact on the possible system response and the fuel consumption of the Diesel engine. These systems are over-actuated and, in order to obtain the best result regarding fuel consumption, require the use of specialized models and controllers.

In the scope of this project, we design a predictive supervisory controller for a delivery van. We intend to show that, by hybridizing such a vehicle and applying a predictive supervisory controller, which considers the vehicle’s exhaust gas aftertreatment system, the fuel consumption can be reduced by 20% compared to the same van using a state-of-the-art conventional propulsion system, while continuing to meet the given emission legislation.

To facilitate the development of the modelling and optimization framework required for designing predictive supervisory controllers, three systems will be considered. This allows for incremental development of the functionality of the modelling and optimization framework, as well as the utilization of parts of the final framework for other projects, as soon as they become available. The three systems are:
1) Diesel engine with exhaust gas aftertreatment system (ATS)
2) Diesel-electric hybrid vehicle with ATS
3) Fuel-cell-electric hybrid vehicle

The research partners FPT Motorenforschung AG and ETH Zurich are currently working on the development of a predictive supervisory controller for vehicle propulsion systems as described in the scope of this project. The funds granted by the BFE-MERFAS subproject SI/501742-01, are used to cover part of the testing expenses occurring at the engine testbench at FPT Motorenforschung AG.

In this report, we present the results of the experimental investigations, partially funded by BFE, for System 1. Furthermore, simulative optimization results for System 2 are presented to assess whether the set goals can be achieved. As the investigation of System 3 is not covered by BFE funds, no results thereof are shown here.

2 Conventional Diesel Engine with Aftertreatment System

We consider the conventional powertrain architecture shown in Figure 1. A Diesel engine provides power to the driveshaft through a clutch and a gearbox. An ATS, consisting of a Diesel oxidation catalyst (DOC), a Diesel particulate filter (DPF), and a selective catalytic reduction (SCR) system, combats pollutants resulting from combustion. The mission is given in the form of engine speed and torque trajectories over time. Consequently, the velocity profile and the gear selection are not optimizable. The engine’s calibration can be changed during operation. Specifically, we consider the start of the fuel injection (SOI), the fuel rail pressure, the position of the guide vanes of the variable geometry turbine (VGT), the position of the exhaust gas recirculation (EGR) valve, and the position of the exhaust flap as engine control inputs that can be optimized. The goal of the supervisory controller is to minimize the amount of fuel consumed while keeping the tailpipe NO_x emissions below the legislative limit. All inputs can be varied continuously within their respective feasible ranges. As the operation of the ATS depends strongly on its temperature, this dynamic must be included in the optimization carried out by the supervisory controller.

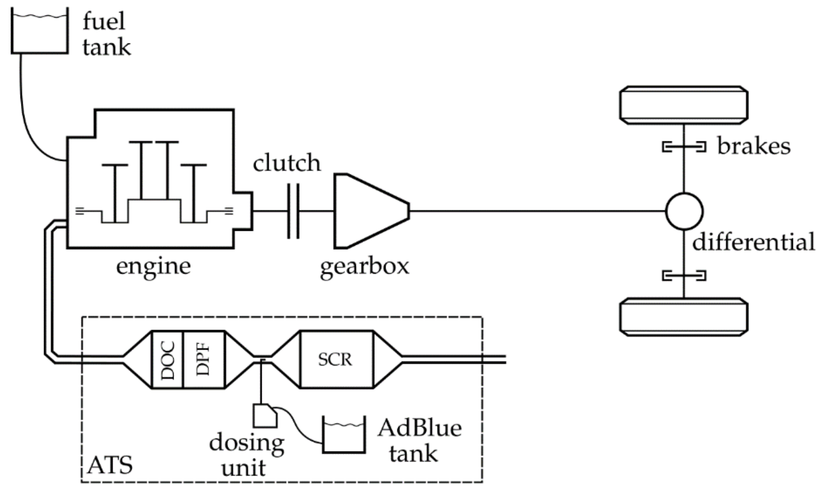

Figure 1 – Powertrain of the conventional Diesel-powered vehicle.

2.1 Preoptimization of Engine Operation

As the engine dynamics are significantly faster than the ATS dynamics, a static engine model was used in this project. Based on design of experiments, around 3000 steady-state measurements were taken, whereby the engine speed and load were varied along with the five engine control inputs. Using these measurements, data-driven black-box models, specifically Gaussian process models, were trained in order to fully describe the engine operation.

Next, as outlined in [1], a preoptimization was carried out, in order to reduce the engine model to the region of interest. The goal thereby is to limit the degrees of freedom that must be set by the supervisory controller by excluding any input combinations that result in an infeasible or suboptimal operation. The preoptimization limits the engine operation to the Pareto front defined by a multi-objective optimization. The objectives considered are minimizing the fuel consumption, minimizing the engine-out NO_x emissions, and maximizing the enthalpy provided to the ATS.

The preoptimized engine model uses look-up elements to characterize the Pareto front. To improve the numerical robustness of the interpolation, a scaled and rotated version of the Pareto front is stored using the variables $J_{\mathrm{X}}^{\mathrm{rot}}$, where $\mathrm{X} \in \{\mathrm{Hd},\ \mathrm{NO_x},\ \mathrm{fuel}\}$. An example of such a Pareto front for a given speed ω_e, torque T_e, and ATS temperature ϑ is shown in Figure 2.

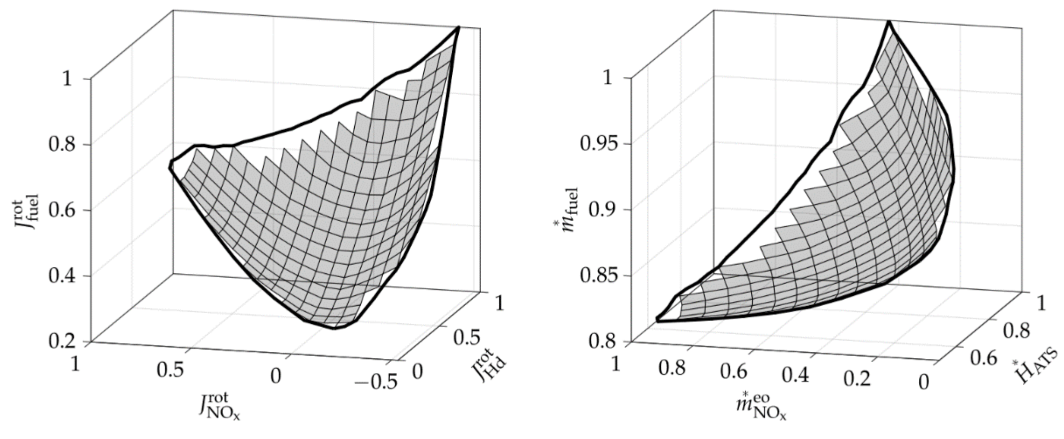

Figure 2 - Exemplary Pareto front at an engine speed of 2000 rpm, an engine torque of 200 Nm, and an ATS temperature of 340 K. The gray surface shows the identified Pareto front, while the solid black lines show the bounds on $J_{NO_x}^{rot}$. On the left the fitted Pareto front described by scaled and rotated values is shown. On the right the fitted Pareto front transferred back to physically meaningful values is shown. The values in the plot on the right were normalized.

As a result of the preoptimization, only the two engine strategy inputs $J_{\mathrm{Hd}}^{\mathrm{rot}}$ and $J_{\mathrm{NO_x}}^{\mathrm{rot}}$ must be set by the supervisory controller, instead of the five engine control inputs, and the feasibility of the engine operation no longer has to be checked, as it is guaranteed by design. The preoptimization therefore greatly simplifies the optimization problem that must be solved by the supervisory controller.

2.2 ATS Models

In the following, three ATS models with different model assumptions are used.

- **two-state ATS model** – This model features two states. A first state is used to capture the thermal dynamics and a second state is used to characterize the ammonia storage of the SCR.
- **one-state best-case ATS model** – This model features a single state to capture the thermal dynamics. The ammonia storage is assumed to be at the set point for the current ATS temperature. The model tends to overestimate the ammonia storage and the NO_x-reduction efficiency.
- **one-state worst-case ATS model** – This model features a single state to capture the thermal dynamics. The ammonia storage is assumed to be at the steady-state for the current ATS temperature. The model tends to underestimate the ammonia storage and the NO_x-reduction efficiency.

While the two-state ATS model is the most accurate of the three, its additional state results in an increased complexity of the optimization. Both one-state models make an assumption regarding the ammonia storage. Which model can better capture the ATS behavior depends on the operation of the ATS, i.e., the ATS temperature and the ammonia storage. While the modeled NO_x-reduction efficiency of the two models differs at low temperatures, they show the same behavior at high ATS temperatures, where the AdBlue injection limit is not active.

Dynamic measurements taken at the testbench were used to identify the model parameters of the thermal ATS models, while simulation results from a high-fidelity ATS model were used to identify the parameters of the chemical ATS models.

2.3 Offline Optimization

Dynamic programming (DP) optimizations were performed using the Dynamic Programming Matlab function dpa extended and updated in the scope of the MERFAS project SI/501643-01 (contract between BFE and ETH). To simplify the calculation and the interpretation of the results, the tailpipe NO_x emissions were included in the objective function, rather than using an additional state and a terminal constraint thereon. The resulting objective is the minimization of

$$J = \left(1 - \mu_{\mathrm{NOx}}^{\mathrm{tp}}\right) \cdot m_{\mathrm{fuel}} + \mu_{\mathrm{NOx}}^{\mathrm{tp}} \cdot m_{\mathrm{NOx}}^{\mathrm{tp}} ,$$

where m_{fuel} is the consumed fuel mass, $m_{\mathrm{NOx}}^{\mathrm{tp}}$ is the emitted tailpipe NO_x mass, and $\mu_{\mathrm{NOx}}^{\mathrm{tp}}$ is the optimization weight on the tailpipe NO_x emissions. For $\mu_{\mathrm{NOx}}^{\mathrm{tp}} = 0$ the most fuel-efficient operation is chosen, whereas $\mu_{\mathrm{NOx}}^{\mathrm{tp}} = 1$ results in the lowest tailpipe NO_x emissions. The DP optimization can be used to analyze the optimal operation under various conditions and for different weights on the tailpipe NO_x emissions and provides a benchmark for supervisory controllers.

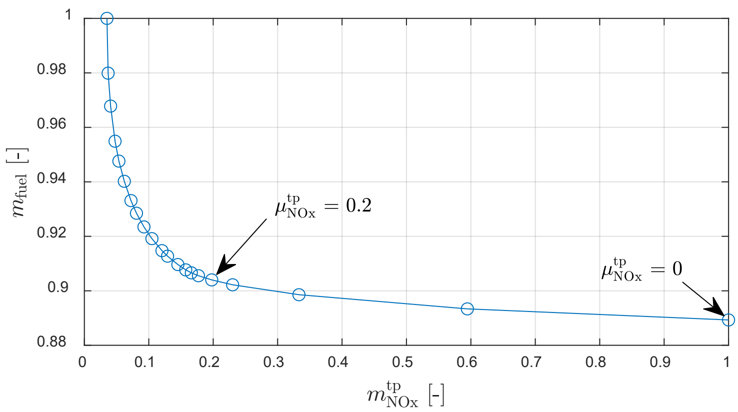

Figure 3 – Simulated Pareto front obtained by a μ_{NOx}^{tp} variation for the world harmonized stationary cycle (WHSC) and an initial ATS temperature of 100°C using the one-state worst-case ATS model. All values were normalized.

Figure 3 shows the trade-off between the fuel consumption and the emitted tailpipe NO_x mass. While the extremes in the fuel consumption differ by around 11%, the variation in the tailpipe NO_x emissions is more pronounced. Comparing the operation with $\mu_{\mathrm{NOx}}^{\mathrm{tp}} = 0$ to that with $\mu_{\mathrm{NOx}}^{\mathrm{tp}} = 0.2$, shows that an 80% reduction in the emitted tailpipe NO_x mass can be achieved with an increase of 1.7% in the fuel consumption.

A more detailed analysis is presented in Figure 4. For $\mu_{\mathrm{NOx}}^{\mathrm{tp}} = 0$ (blue), the engine-out NO_x mass flow is high throughout the cycle. During the initial phase, when the ATS is still cold, these emissions cannot be converted and are emitted to the atmosphere. This causes a sharp rise in the emitted tailpipe NO_x emissions. As $\mu_{\mathrm{NOx}}^{\mathrm{tp}}$ is increased, the engine-out NO_x emissions at the beginning of the cycle are reduced first, which results in the strongest tailpipe NO_x reduction per increase in the fuel consumption. As tailpipe NO_x emissions are decreased further, the resulting fuel penalty increases strongly, see Figure 3. For $\mu_{\mathrm{NOx}}^{\mathrm{tp}} = 1$ (green), the engine-out NO_x emissions are minimized throughout the cycle. The influence of $\mu_{\mathrm{NOx}}^{\mathrm{tp}}$ on the ATS temperature is less pronounced and only when $\mu_{\mathrm{NOx}}^{\mathrm{tp}} = 1$, can a significant rise in the ATS temperature be observed.

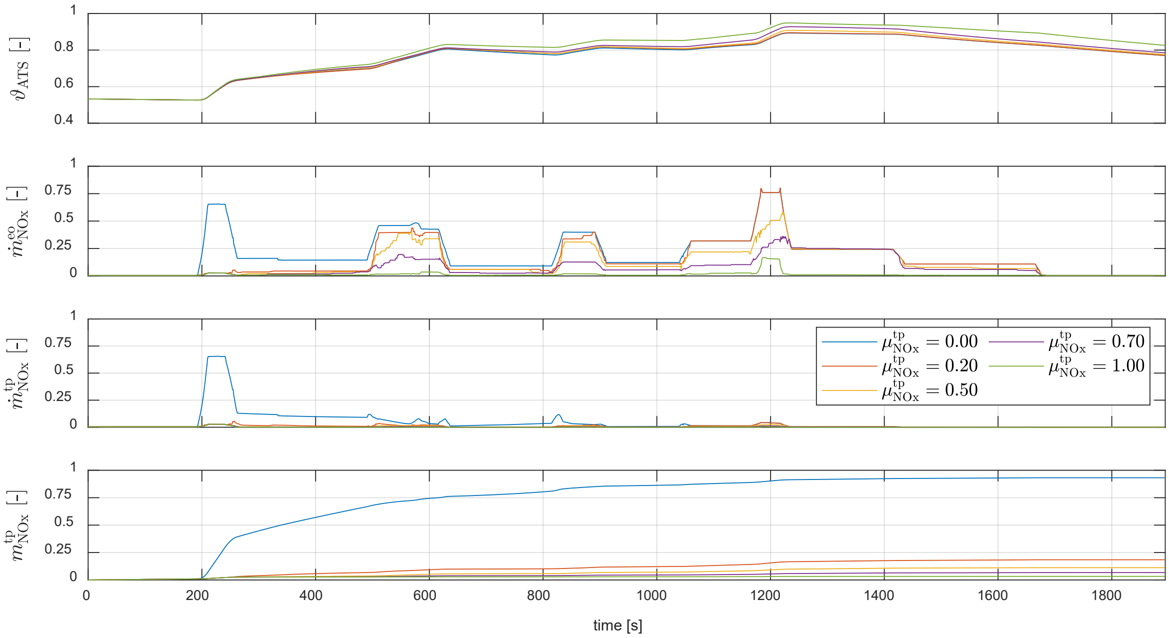

Figure 4 - Optimal operation for the WHSC cycle and an initial ATS temperature of 100°C using the one-state worst-case ATS model. Shown are the ATS temperature, the engine-out NO_x mass flow, the tailpipe NO_x mass flow, and the emitted tailpipe NO_x mass. All values were normalized.

2.4 Feedforward Control

To validate the optimization result shown in the previous section, experimental tests were carried out at the testbench. In order to create reproducible test conditions, each cycle was started with an empty ammonia storage and an initial temperature of 100°C. These conditions were chosen, because the system can be brought back to the initial state reliably and efficiently after each test cycle and because they represent the important case of a cold start.

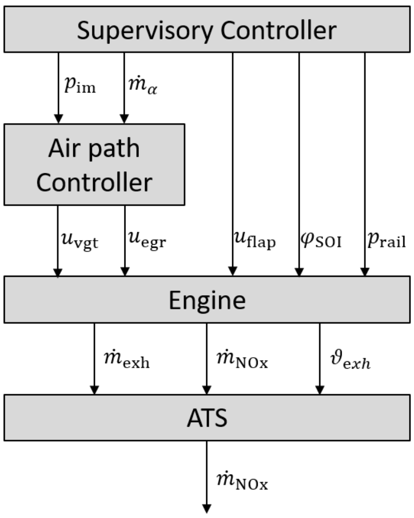

Figure 5 – Control structure for experiments.

The control structure used for these tests is visualized in Figure 5. The engine inputs for the exhaust flap u_{flap}, the injection timing φ_{SOI}, and the fuel rail pressure p_{rail} are provided directly by the supervisory controller. For the control of the air path, the existing air-path controller is used and the supervisory controller provides the set points for the intake pressure p_{im} and the air mass flow $\dot{m}_{\alpha}$.

To check that the experiments are repeatable, each measurement was repeated three times and the results are compared, see Figure 6. Even though static engine maps were used, the engine outputs are generally captured accurately. At high engine torques (210-240 s and 1180-1220 s) the exhaust enthalpy was overestimated. During both segments the measured value gradually approaches the value from the static engine maps, which suggests that this is likely caused by the dynamic introduced by the thermal inertia of the exhaust piping which is not considered in the model.

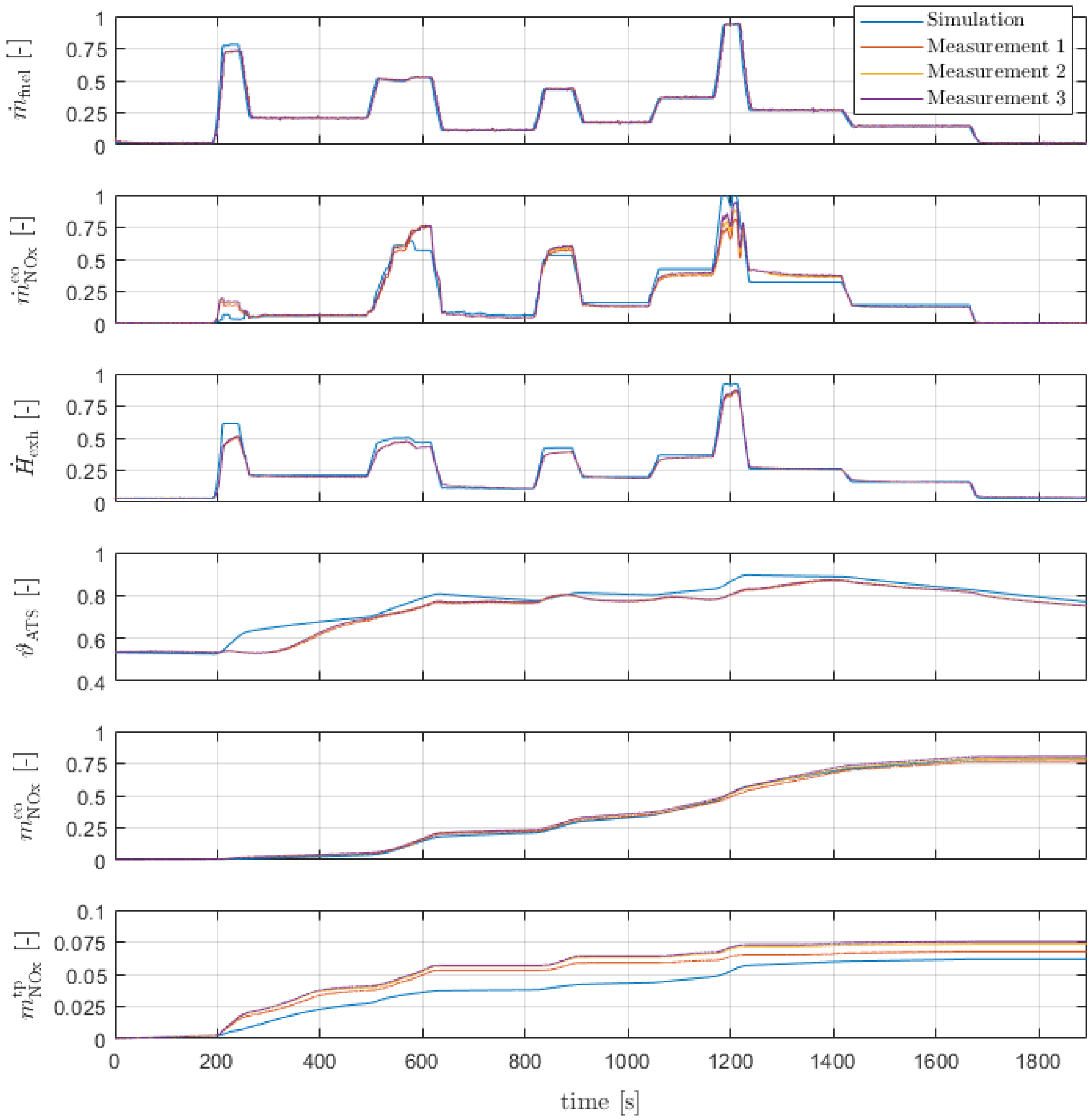

Figure 6 – Experimental result for the WHSC with an initial ATS temperature of 100°C and the two-state ATS model. The plots show the simulation results (blue), as well as the experimental results from three repetitions of the measurement (red, yellow, and purple). Shown are the fuel mass flow, the engine-out NO_x mass flow, the exhaust enthalpy, the ATS temperature, the engine-out NO_x mass, and the emitted tailpipe NO_x mass. All values were normalized.

The ATS temperature and the emitted tailpipe NO_x mass show that the repeatability of the experiment is guaranteed and that there is a non-negligible offset from the simulation. At 210 s, during the first load peak, the simulation shows a sharp rise in the ATS temperature which is not observable in the measured ATS temperature. The overestimation of the exhaust enthalpy by the simulation model would explain a slower rise in the measured ATS temperature, but not an almost stationary ATS temperature. The observed behavior can be attributed to the axial temperature distribution in the ATS, which is not captured by the model. While the model accurately captures the emitted engine-out NO_x emissions, the mismatch in the ATS temperature combined with the modelling error of the ATS chemical model result in a mismatch of the emitted tailpipe NO_x.

Figure 7 shows a comparison of the results obtained by setting the NO_x limit to the emitted tailpipe NO_x mass obtained using today's engine calibration (Euro 6, step D), which was used as the reference in the following. As a result of the optimized operation, the ATS performance was improved, and much more engine-out NO_x could be emitted at a limited increase in the tailpipe NO_x emissions. While the simulation and the measurement consistently match quite well for the consumed fuel mass and the engine-out NO_x mass, the mismatch in the emitted tailpipe NO_x mass varies significantly depending on the ATS models. The one-state best-case ATS model underestimates the emitted tailpipe NO_x mass considerably, as its assumption on the ammonia storage is not well-suited to the case considered. The one-state worst-case ATS model is better suited and the resulting mismatch in the emitted tailpipe NO_x mass is significantly smaller. The best result, however, is achieved by the two-state ATS model.

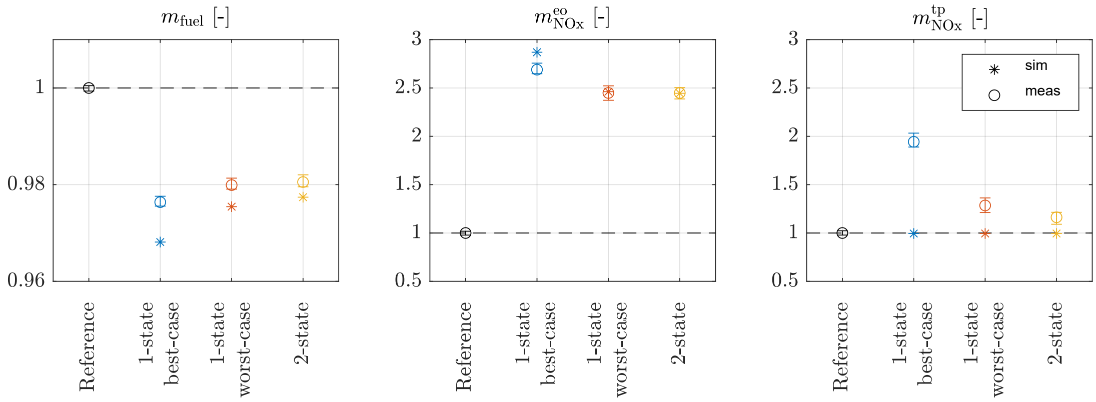

Figure 7 – Comparison of the results obtained using the different ATS models to determine the optimal engine operation for the WHSC with an initial ATS temperature of 100°C. Simulation results are represented by an asterisk. The averaged measured value is represented by a circle with bars representing the minimum and maximum measured value. Shown are normalized values for the consumed fuel mass, the engine-out NO_x mass, and the emitted tailpipe NO_x mass.

The model used by an online optimization-based controller must be efficient to evaluate and should capture the underlying trends. Therefore a one-state ATS model is used in the following. The NO_x-reduction efficiency map is retuned to better fit the measured values. The new map lies between the worst-case and the best-case map used in this section for intermediate ATS temperatures and returns a lower, more realistic NO_x-reduction efficiency for high ATS temperatures. To compensate for the observed model mismatch, the supervisory controller should incorporate feedback control.

2.5 Real-time-capable Optimization Method

The computational time required to solve the DP optimization presented in the previous section is too high for real-time optimization in a predictive supervisory controller. In this section, we present a real-time-capable optimization method, which solves the optimal control problem reformulated as a nonlinear program (NLP) using direct methods, as outlined in [2].

Direct methods can only be used if the model equations are continuously differentiable. This requirement is not fulfilled if the look-up elements used to characterize the preoptimized engine operation are evaluated using linear interpolation, as was done in the previous section. We therefore introduced continuously differentiable look-up elements that use a piecewise quadratic interpolant with a continuous first derivative to characterize the preoptimized engine operation. Next, the OCP is discretized in time and an NLP is formulated. Multiple shooting is used to discretize the ATS temperature state in order to account for the nonlinear dependencies on the ATS temperature. Single shooting is used to discretize the emitted tailpipe NO_x mass state as none of the model equations depend on the emitted tailpipe NO_x mass. The NLP is solved using IPOPT [3].

A drawback of using a direct method is that there is no global optimality guarantee for nonconvex problems such as the one considered here. To check the convergence to the global optimum and the quality of the solution obtained from the NLP optimization, it was compared to a benchmark obtained using DP. A comparison of the trajectories resulting from the DP and the NLP optimizations for the nonroad transient cycle (NRTC) and an initial ATS temperature of 100°C showed no discernible difference. Upon closer inspection, see Table 1, we found that the NLP solution fulfilled the constraint on the emitted tailpipe NO_x mass exactly and that the consumed fuel mass was even 0.049% lower than that of the DP solution. This can be attributed to the error introduced by the state and input discretization during the DP optimization. While this example does not prove that the NLP solver converges to the global optimum in general, it indicates that the resulting solution is of a high quality. Furthermore, the NLP optimization was found to be significantly faster than real-time, making it a viable option for online optimization.

Table 1 - Comparison of the DP and NLP optimization results for the NRTC and an initial ATS temperature of 100°C. Shown are the computation time, the consumed fuel mass, the engine-out NO_x mass, and the emitted tailpipe NO_x mass. The results of the DP optimization were used for the normalization. The computation times reported were obtained on a PC with a 2.8 GHz quad-core processor and 32 GB of RAM.

Method	t_{calc}	m_{fuel} [%]	$m^{eo}_{NO_x}$ [%]	$m^{tp}_{NO_x}$ [%]
DP	15.8 h	100	100	100
NLP	23.4 s	99.951	100.943	100.000

2.6 Predictive Supervisory Controller

When the solution obtained in the previous section is applied at the testbench in a feedforward manner, an offset is observable due to model mismatch. To guarantee, that the NO_x limit is respected during operation of the real system, an online controller with feedback is required. The structure of the controller developed in this work is shown in Figure 8. The predictive supervisory controller, contains two layers. In both layers, an optimization problem is solved to determine the optimal operation over the prediction horizon.

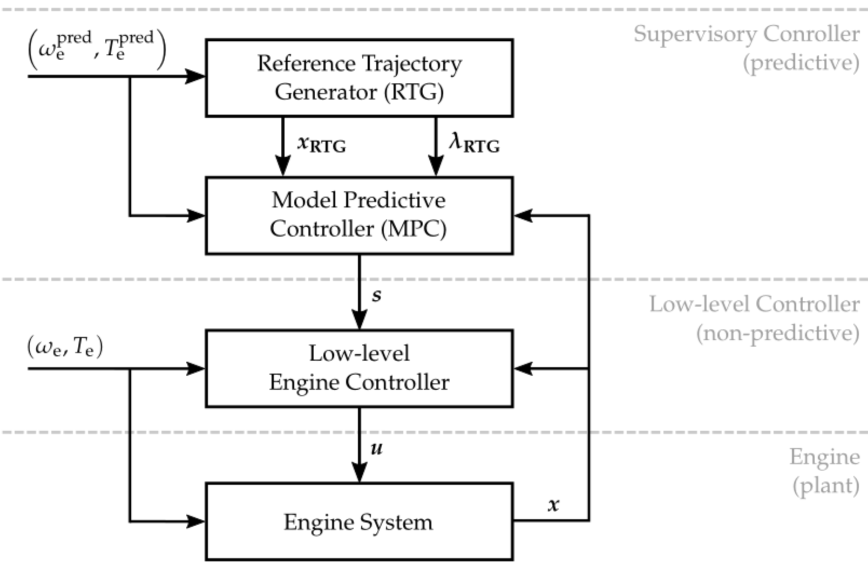

Figure 8 - Controller structure consisting of a predictive supervisory controller that passes a strategy input vector s to a non-predictive low-level engine controller that sets the engine control input vector u. The vector of measured system states x is used as feedback.

The task of the RTG is to optimize the operation of the engine system over the entire mission and provide reference trajectories that the MPC will follow. In this work, the predictive information is considered to be of a high quality, i.e., there is limited benefit in updating the reference trajectories during the mission. However, the RTG could be updated if a change in the mission is detected or a significant offset of the current states from their respective reference is detected.

The task of the MPC is to correct for errors introduced by model mismatch and misprediction in an optimal fashion. To achieve this, an OCP is solved at every update time and the resulting strategy inputs are passed to the low-level controller. The OCP is initialized with the current ATS temperature and emitted tailpipe NO_x mass, and the terminal state constraints are chosen such that the system is brought back to the reference by the end of the prediction horizon. To limit the computational burden of the MPC, its prediction horizon is chosen significantly shorter than that of the RTG.

Details on the implementation of the supervisory controller can be found in [2].

2.7 Experimental Results

Figure 9 shows that the emitted tailpipe NO_x mass exceeds the limit by 27.9% when the MPC is deactivated, i.e., no feedback control is available. When the MPC is activated, the effect of the model mismatch is compensated for and the reference trajectory for the emitted tailpipe NO_x mass is tracked. During the first 500 s of the mission even the operation with MPC exceeds the reference for emitted tailpipe NO_x mass. As shown in [2], this could be attributed to a loss of controllability when following the reference requires an engine operation that is not possible with the real system. We conclude that the predictive supervisory controller showed good reference tracking behavior when the system bounds allowed for sufficient controllability. When the reference obtained from the RTG cannot be tracked by the real system due to loss of controllability, the supervisory controller continues to track the reference as well as the real system allows.

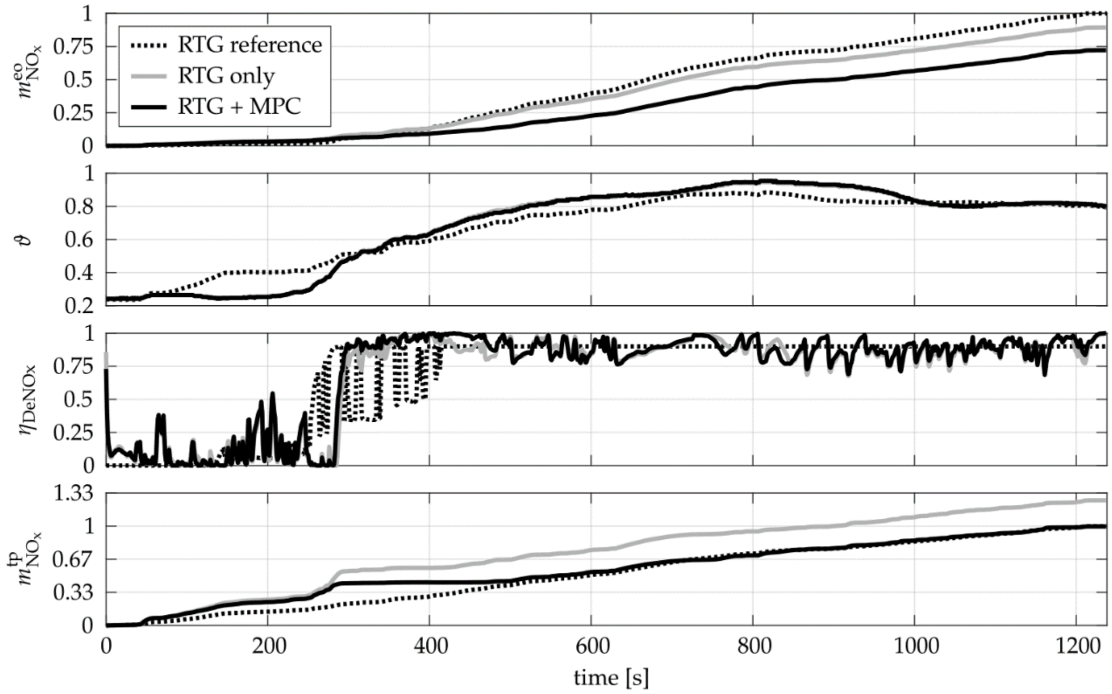

Figure 9 - Results for the NRTC with an initial ATS temperature of 100°C. Shown are the engine-out NOx mass, the ATS temperature, the NO_x-reduction efficiency of the ATS, and the emitted tailpipe NO_x mass. The optimization result obtained from the RTG is labeled RTG reference, the measured operation using only the RTG is labeled RTG only, and the measured operation using the full predictive supervisory controller is labeled RTG+MPC. All values were normalized.

Figure 10 shows how the predictive supervisory controller can adapt to different conditions and tailpipe NO_x limits. The result on the left corresponds to that shown in Figure 9. The measured operation obtained with the predictive supervisory controller shows that the tailpipe NO_x limit was respected and that the fuel consumption could be reduced by 1.1%.

The comparison in the middle of Figure 10 corresponds to the case where the same tailpipe NO_x limit as before was set, but the initial ATS temperature was 300°C resulting in a much higher average NO_x-reduction efficiency. The operation obtained with the fixed engine calibration resulted in a final emitted tailpipe NO_x mass 46% below the limit. The fixed engine calibration is too conservative for this mission and fuel could have been saved by adapting it. This was achieved by the predictive supervisory controller, which exploited the fact that the tailpipe NO_x limits were less restrictive, resulting in a 2.0% reduction in the fuel consumption while exceeding the tailpipe NO_x limit by 1.0%.

The comparison on the right of Figure 10 corresponds to the case where the initial ATS temperature was 100°C but the tailpipe NO_x limit was reduced to 0.66. The operation obtained with the fixed engine calibration reached a final emitted tailpipe NO_x mass 53% above the limit. The fixed engine calibration is too optimistic for this mission. The predictive supervisory controller on the other hand adapted to the new tailpipe NO_x limit and only exceeded it by 1.7%. This was achieved at the cost of a 1.2% increase in fuel consumption.

Robustness of the predictive supervisory controller toward mispredictions can be achieved by using equivalence factors as the output from the predictive supervisory controller and solving a static optimization problem online to determine the engine control inputs in the low-level engine controller.

The results for the operation with mispredictions are shown in Figure 11. For all experiments, the NRTC was followed during the experiment. The NRTC consists of seven segments that describe the operation of different non-road applications [4]. The first misprediction case was obtained by filtering the NRTC using a low-pass filter with a cut-off frequency of 0.01 Hz and represents the case where only averaged information about the upcoming mission is available. The second misprediction case was obtained by rearranging the individual segments of the NRTC and represents the case where the timing of the predictive information is wrong.

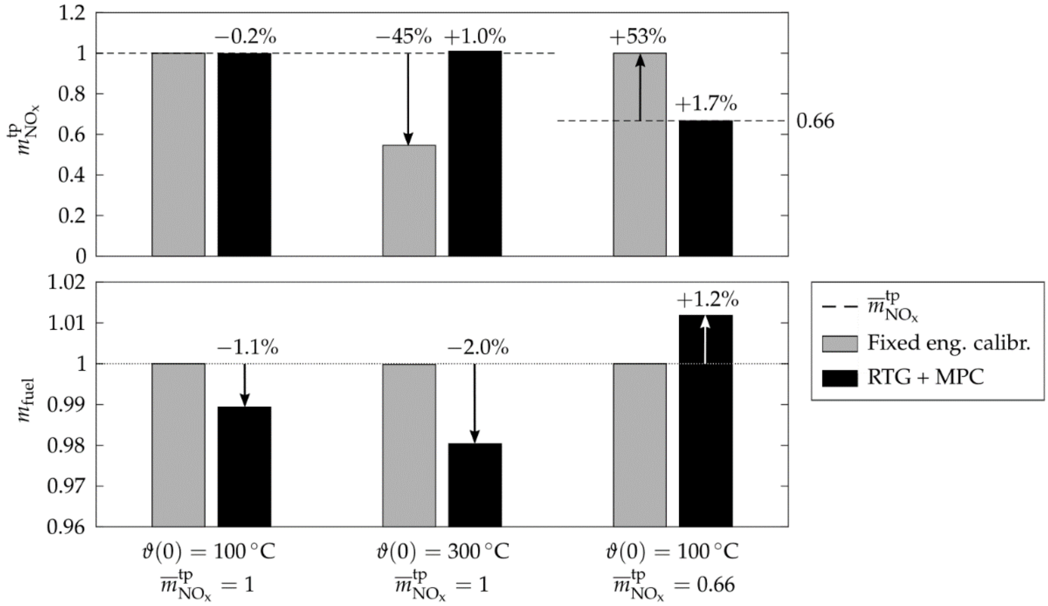

Figure 11 – Comparison of the resulting operation for the NRTC for different initial ATS temperatures $\vartheta(0)$ and tailpipe NO_x limits $\overline{m}^{tp}_{NO_x}$. The results obtained with the fixed engine calibration of the stock ECU are shown in gray, while the results obtained with the predictive supervisory controller are shown in black. All values were normalized w.r.t. the operation with the fixed engine calibration for $\vartheta(0) = 100℃$ and $\overline{m}^{tp}_{NO_x} = 1$.

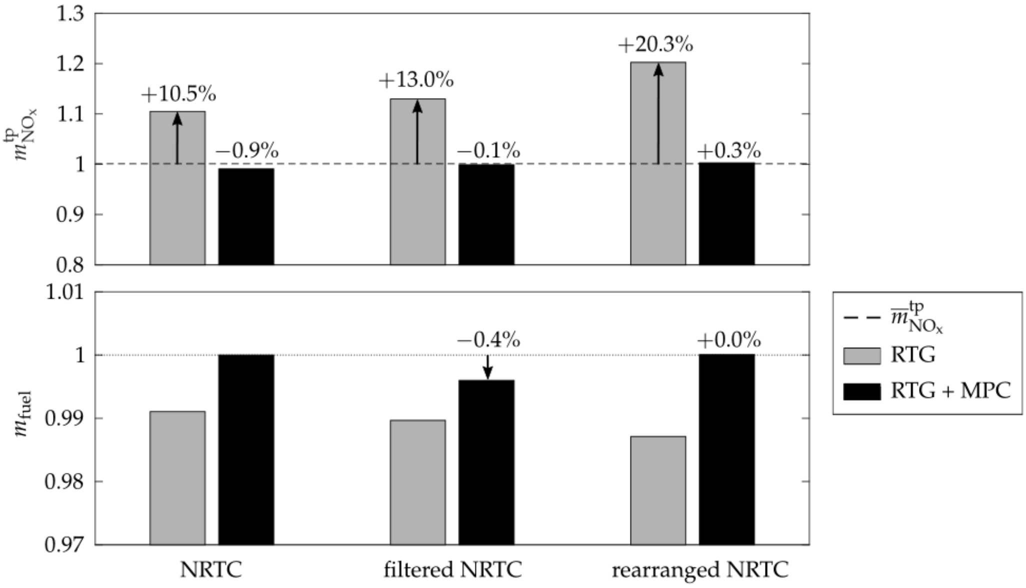

Figure 10 - Comparison of the operation for different misprediction cases. The results obtained without feedback from the MPC are shown in gray, while the results obtained with the full predictive supervisory controller are shown in black. The emitted tailpipe NO_x mass is normalized w.r.t. the limit, while the fuel mass is normalized w.r.t. the operation with the full predictive supervisory controller for the case without misprediction.

The effect of misprediction can be analyzed by first considering the operation without feedback from the MPC. For the case without misprediction, the error of 10.5% in the emitted tailpipe NO_x mass stems solely from model mismatch. For the cycles with misprediction, the error increased to 13.0% for the filtered NRTC and to 20.3% for the rearranged NRTC.

When feedback was introduced via the MPC, the predictive supervisory controller exceeded the tailpipe NO_x limit by no more than 0.3% for all considered cases. This result indicates that the supervisory controller is robust to mispredictions. Furthermore, the increased feedback control action required to reach the tailpipe NO_x target for the cases with misprediction did not result in an increase in fuel consumption.

In this section, a non-road mission was considered. The motivation for this is that the mission features heavier transients and is likely more challenging than typical on-road missions. This highlights the adaptability of the predictive supervisory controller to arbitrary missions. Similar investigations for the world harmonized transient cycle (WHTC) show that at equivalent NO_x emissions, the fuel reduction potential is negligible, but the adaptability to different conditions and tailpipe NO_x limits as demonstrated in Figure 10 remains.

In summary, the predictive supervisory controller was shown to adapt well to different missions, initial ATS temperatures, NO_x limits, and mispredictions. The preoptimization method and the resulting predictive supervisory controller were patented by FPT Motorenforschung AG in [5].

3 Diesel-Electric Hybrid Vehicle

We consider a parallel-hybrid powertrain in P3 configuration (Figure 12). The electric motor is connected to the torque splitter via a fixed-transmission-ratio gearbox and draws power from the battery via a DC-DC converter. The Diesel engine is connected to the torque splitter via a clutch and a six-speed automated gearbox. The ATS consists of a Diesel oxidation catalyst (DOC), a Diesel particulate filter (DPF), and a selective catalytic reduction (SCR) system. In addition to the engine strategy, the supervisory controller has to set the clutch position (engaged/disengaged), the selected gear of the engine gearbox, and the torque split. The goal of the supervisory controller is to minimize the amount of fuel consumed, while achieving a charge-sustaining operation and keeping the tailpipe NO_x emissions below the legislative limit. As both continuous inputs and discrete inputs need to be considered, a mixed-integer problem results. Due to their combinatorial nature, problems of this class are notoriously hard to solve.

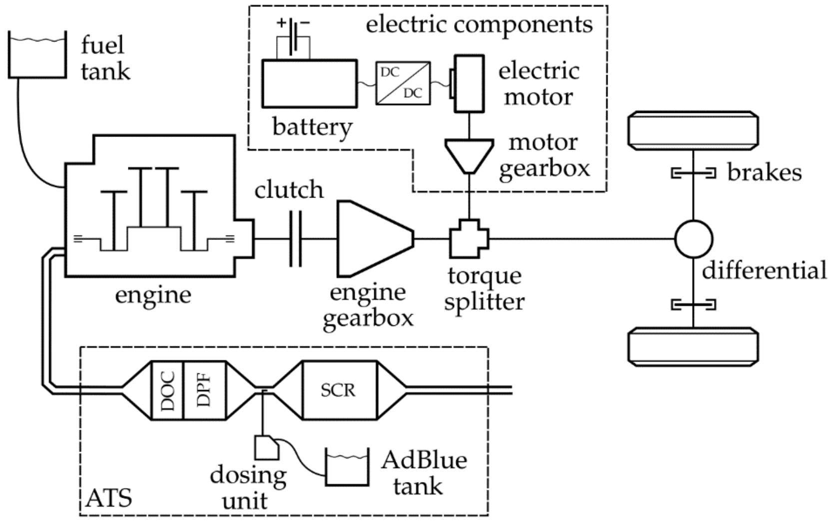

Figure 12 - Powertrain of the considered Diesel-electric hybrid vehicle.

The supervisory control design for the hybrid electric vehicle (HEV) was split into three phases as outlined in the report to the BFE MERFAS project SI/501643-01 (contract between BFE and ETH). First, a Diesel engine with a fixed engine calibration was considered and NO_x emissions were neglected. The goal of this phase was to develop an optimal energy management controller. The corresponding results were published in [6] and resulted in the patent [7]. Second, a Diesel engine with a fixed engine calibration was considered and the ATS and the NO_x emissions were included in the optimization. An energy and emission management controller was developed. The corresponding results were published in [8] and resulted in the patent [9]. Third, the full optimization problem including an engine with a variable engine calibration was considered. In this report, only the results for this final phase are shown.

Further analysis and testing of the optimization algorithm outlined in [8] has shown that cases exist where no robust convergence can be achieved, and the optimization method was not employed further. Therefore, no real-time-capable optimization method is available and no investigations regarding online control could be performed. Nevertheless, the simulative offline optimization results obtained using DP are presented in the following.

3.1 Electric Component Model

We use the model of the electrical components outlined in [6]. It assumes a constant efficiency for the motor gearbox and the DC/DC converter, an efficiency map spanned over speed and torque for the electric motor and an equivalent circuit model for the battery.

3.2 Offline Optimization

In [1], the optimal operation of the HEV with different degrees of freedom is analyzed. The results are shown in Figure 13. The case of the conventional vehicle with a fixed engine calibration (square marker) is considered as the baseline. Different missions were considered to investigate the effect of the mission on the benefit of optimizing the individual degrees of freedom.

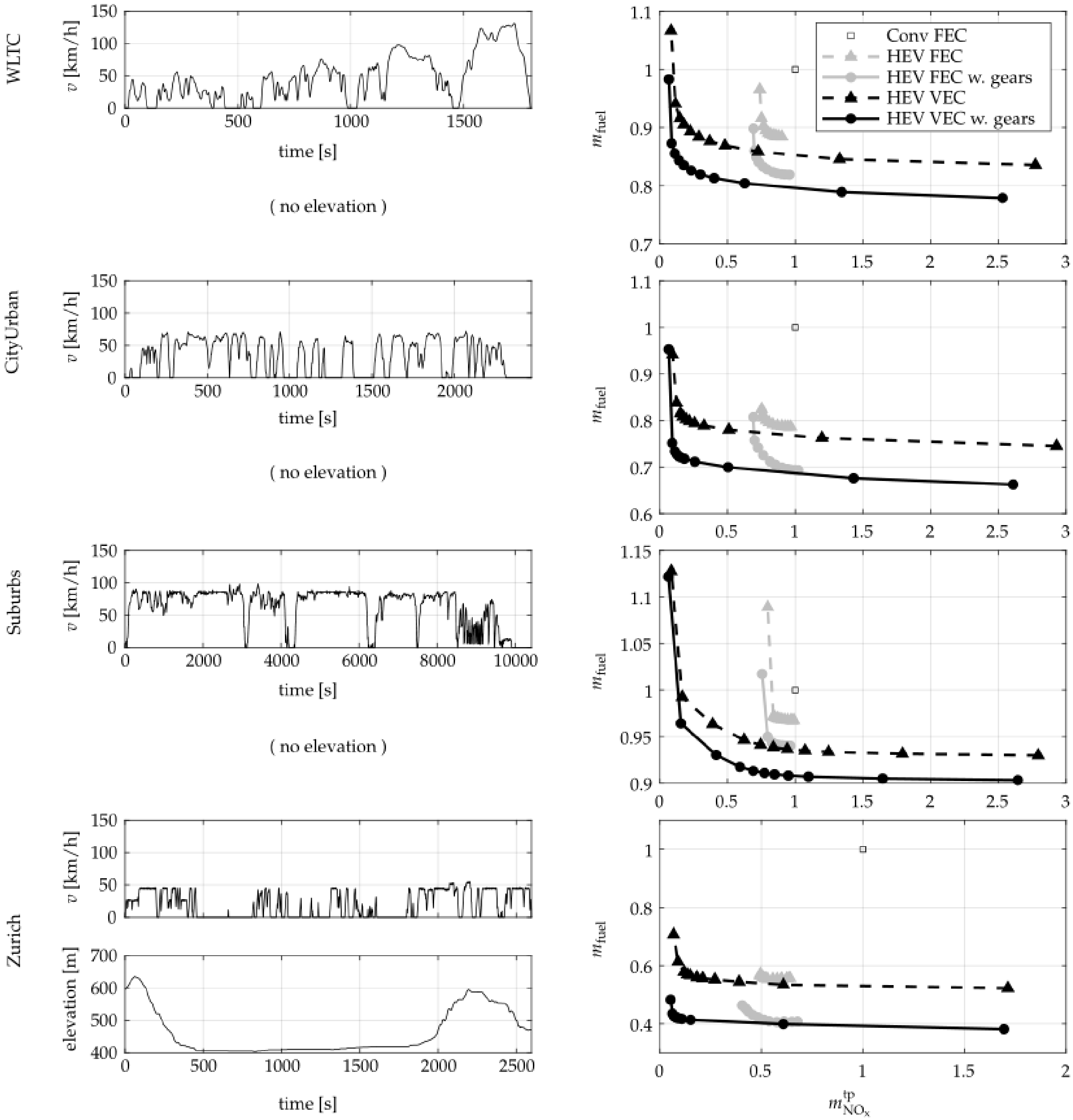

Figure 13 - Optimal operation of the HEV for different degrees of freedom. Conv denotes the conventional vehicle, HEV denotes the hybrid electric vehicle, FEC denotes a fixed engine calibration, VEC denotes a variable engine calibration, and w. gears denotes optimized gear selection and engine on/off decision. The considered driving missions are shown on the left with the resulting trade-offs between fuel consumption and emitted tailpipe NO_x mass shown on the right. An initial ATS temperature well below the light-off temperature was used for all driving missions. All values were normalized.

The potential for fuel consumption reduction through hybridization (HEV FEC) is strongly dependent on the vehicle mission. Missions with frequent braking phases or pronounced elevation profiles offer ample opportunity for recuperation. As a result, through hybridization alone, the fuel consumption on the world-wide harmonized light vehicles test cycle (WLTC), the CityUrban driving mission, and the Zurich driving mission, can be reduced by roughly 12%, 21%, and 45%, respectively, when the NO_x emission limit is set to that of Conv FEC. For the Suburbs driving mission, which features prolonged operation at higher velocity and does not offer any significant recuperation phases, the achievable reduction in the fuel consumption is only 3%.

For a constant requested power, the fuel consumption increases with a rising engine speed, while the engine-out NO_x emissions remain approximately constant. As a result, the effect of the gear selection on the fuel consumption is more pronounced than its effect on the NO_x emissions. The achievable advantage through gear optimization (HEV FEC w. gears) is larger for missions with low and/or frequently changing vehicle velocities. The fuel consumption is also lower as the gear optimization allows the engine drag losses to be avoided during fuel cut-off phases by decoupling the engine from the drivetrain.

While optimizing the torque split, the gear selection, and the engine on/off decision enables a trade-off between the fuel consumption and NO_x emission, this region is drastically extended for all missions considered if additionally VEC is enabled (HEV VEC and HEV VEC w. gears). Most notably, the region with very low NO_x emissions can only be reached if the engine operation can also be optimized by the supervisory controller.

In summary, the results show that while hybridization on its own offers the possibility to significantly reduce the fuel consumption, the potential to reduce the vehicle's tailpipe NO_x emissions is limited. When additionally VEC is enabled, a further, but limited reduction in the fuel consumption is possible, while the tailpipe NO_x emissions can be reduced drastically.

4 Conclusion and Outlook

In this project, a predictive supervisory controller for a conventional Diesel-powered delivery van was developed and tested at the engine testbench. It was shown to reduce the fuel consumption by 1.1% at equivalent tailpipe NO_x emissions for the NRTC when compared to the operation with a fixed engine calibration. Further, the controller's robustness to different missions, initial ATS temperatures, NO_x limits, and mispredictions was demonstrated.

For the HEV, an online predictive supervisory controller, could not be realized, due to the lack of a real-time-capable optimization method to solve the resulting complex mixed-integer optimization problem. However, an offline potential analysis was shown using a DP optimization. It was shown, that the targeted reduction in fuel consumption of 20% compared to a conventional vehicle with a fixed engine calibration could indeed be within reach for the WLTC. For urban driving cycles, the expected potential is higher, while for highway cycles it is lower.

For FPT Motorenforschung AG, the calculated optimal solutions provided new insights into the optimal operation of the considered powertrain and furthered the understanding of how to optimally operate similar powertrains.

Based on this project, there are four avenues for future research. First, the predictive supervisory controller could be applied to series production conventional vehicles. The focus should lie on the integration of the optimization method to embedded systems and on obtaining accurate and reliable predictive information for the supervisory controller. Second, further research into the development of a predictive supervisory controller for HEVs could be conducted. A possible approach could be to use a heuristic controller to set the integer control variables, thereby removing them from the optimal control problem that needs to be solved online. Third, simpler, potentially non-predictive supervisory controllers could be developed. During the development, their performance should be assessed by comparing them to the benchmark set by the method presented in this work in order to quantify the resulting suboptimality. Fourth, the developed methodology could be used to develop a tool for optimal component sizing.

References

[1] J. Ritzmann, O. Chinellato, R. Hutter and C. Onder, "Optimal Integrated Emission Management through Variable Engine Calibration," *Energies,* vol. 14, no. 22, 2021.

[2] J. Ritzmann, C. Peterhans, O. Chinellato, M. Gehlen and C. Onder, "Model Predictive Supervisory Control for Integrated Emission Management of Diesel Engines," *Energies,* submitted.

[3] A. W. Wächter, "Interior point methods for large-scale nonlinear programming with applications in process systems engineering," *Pittsburgh, PA, USA: Carnegie Mellon University,* 2002.

[4] J. Ettl, H. Bernhardt, K. Thuneke, P. Emberger and E. Remmele, "Transient emission and fuel consumption measurements," *Landtechnik,* vol. 71, pp. 44-54, 2016.

[5] J. Ritzmann, O. Chinellato, R. Hutter and C. Onder, "Method for powertrain modelling and controlling of the modelled powertrain". Patent pending.

[6] J. Ritzmann, A. Christon, M. Salazar and C. Onder, "Fuel-optimal power split and gear selection strategies for a hybrid electric vehicle," *SAE Technical Paper,* 2019.

[7] J. Ritzmann, O. Chinellato, A. Christon, S. Mauro and C. Onder, "A method and a system for controlling a vehicle on a mission". Patent EP3756963, 30 12 2020.

[8] J. Ritzmann, G. Lins and C. Onder, "Optimization method for the energy and emissions management of a hybrid electric vehicle wih an exhaust aftertreatment system," *IFAC-PapersOnLine,* vol. 53.2, pp. 13797-13804, 2020.

[9] J. Ritzmann, O. Chinellato, G. Lins, S. Mauro and C. Onder, "A method and a system for controlling a vehicle on a mission". Patent WO2021229526, 18 11 2021.